Parallel molecular dynamics simulations for the oxidation of an aluminium nanocluster

1998 J. Phys.: Condens. Matter 10 11449

(http://iopscience.iop.org/0953-8984/10/49/031)

J. Phys.: Condens. Matter **10** (1998) 11449–11458. Printed in the UK PII: S0953-8984(98)96505-5

Parallel molecular dynamics simulations for the oxidation of an aluminium nanocluster

S Ogata† and T J Campbell‡

† Department of Applied Sciences, Yamaguchi University, 2557 Tokiwadai, Ube 755-8611, Japan

‡ Concurrent Computing Laboratory for Materials Simulations, Department of Physics and Astronomy, Department of Computer Science, Louisiana State University, Baton Rouge, LA 70803, USA

Received 4 June 1998

Abstract. The oxidation of an Al nanocluster with radius 100 Å placed in oxygen gas at room temperature is investigated by performing molecular dynamics simulations on parallel computers. The simulations take into account the effects of dynamic charge transfer between Al and O on the basis of electronegativity-equalization principles. We thereby find that molten surface oxides are saturated to depths of 28–33 Å; this saturation is accompanied by depletion of oxygen near the cluster in the environment. Upon quenching the cluster further in oxygen gas, amorphous surface oxides with depths ∼38 Å are formed. The microscopic structures of the amorphous oxides are characterized.

1. Introduction

Metals and semiconductors oxidize easily in the atmosphere; this oxidization results in the alteration of their mechanical and physical properties [1]. Passivation [1] is one of the engineering techniques used to control oxidation, and it is applicable to Al; we may coat a surface of Al with protective surface oxides (Al_2O_3) by exposing it to a highly oxidizing environment [2]. Aluminium nanoclusters of radii 50–200 Å also form layers of amorphous Al_xO_y with depths of 20–30 Å in low-density oxygen gas at room temperature [3–5]. We can utilize such passivated Al nanoclusters in various applications [5, 6]. Passivated nanophase Al [6], produced by consolidating the passivated Al nanoclusters, may have novel properties because of its nanometre-sized complex structures. Despite their intrinsic significance, no reliable theory on the detailed mechanisms of the oxidation and passivation of such nanoclusters exists. Outstanding problems include investigation of why the oxidation ceases before completion, and the characterization of microscopic structures of the amorphous surface oxides. Computer simulations for the oxidation of an Al nanocluster will offer invaluable information for use in addressing these problems.

Recent advances in parallel computers and simulation algorithms have made it possible to perform large-scale molecular dynamics (MD) simulations of less-ionic materials [7]. Using empirical short-range interatomic potentials, one can perform simulations of materials with sizes of the order of 100 Å. However, no realistic simulations have been performed for chemical reactions such as oxidation, for nanometre-sized materials. For the oxidation of an Al nanocluster, the difficulty in performing large-scale simulations stems from the

0953-8984/98/4911449+10$19.50

ionic nature of Al and O; substantial charge transfer takes place between Al and O atoms due to their difference in electronegativity [1]. The amount of charge transfer between the pair depends on the atomic configuration of the material, since the pair interacts with all of the other atoms via the long-range Coulomb potential. In the MD simulations, therefore, a highly efficient algorithm for fast calculation of the Coulomb interactions is required for determining atomic charges dynamically.

In this paper we report on variable-charge MD simulations for the oxidation of an Al nanocluster (radius: 100 Å) exposed to oxygen gas; both atomic oxygen and molecular oxygen are considered. We find that the oxidation starts from the surface of the cluster, accompanied by substantial charge transfers in the oxidizing region. The surface oxides melt because of their high temperatures (>2000 K), stemming from binding-energy release in the oxidation reaction. The surface oxides are saturated to depths of 28–33 Å, while the density of oxygen in the oxides varies depending on the setting of the simulation. At the saturation stage, oxygen in the environmental region near the cluster is depleted. By quenching the cluster in oxygen gas, we obtain amorphous surface oxides with depths ∼38 Å. The microscopic structures of the amorphous surface oxides are investigated through vibrational densities of states, and local analyses.

2. Parallel molecular dynamics simulations

A fcc crystalline Al sphere with radius $r = 100$ Å composed of 252 158 particles is placed at the centre ($x = y = z = 0$) of the MD box (800 Å × 800 Å × 800 Å). A total of 530 720 oxygens are distributed randomly in the range $r = 110$–400 Å in the form of either atoms (O_1) or molecules (O_2). Hence, the averaged density of oxygens is 0.0020 $Å^{-3}$ in the environment; it is about 40 times as large as that for the standard state (1 atm and 300 K). A spherical hard wall with $r = 400$ Å inscribing the MD box is assumed for confinement. The initial temperatures of both the Al cluster and the environmental oxygens are set to 300 K. The velocity Verlet algorithm, with multiple time steps of 1 fs for short-range forces and 20 fs for long-range forces, is adopted for the time integration of the positions and the velocities in the MD simulations [8]. Canonical MD simulation, in which the temperature of the whole system is fixed at 400 K by means of a Nosé–Hoover thermostat [9], is performed for the case of O_2 in addition to the microcanonical MD.

We adopt the empirical interatomic potentials (ES+) developed by Streitz and Mintmire [10] for aluminium and alumina materials. In the MD simulations with ES+, the atomic charges are determined dynamically as a function of the atomic configuration on the basis of generalized electronegativity-equalization principles. For fast computations of the resulting Coulomb interactions, we implement the fast multipole method (FMM) [11] with a useful extension for stress calculations; multipoles up to the quadrupole are included in the FMM. We note that use of ES+ reproduces well the ground-state properties of Al and α-Al_2O_3 crystals, including the cohesive energies, elastic constants, phonon spectra, and surface energies [10]. The dissociation energy of an O_2 molecule in vacuum calculated using ES+, on the other hand, is about 60% of the experimental value.

The present MD code is highly parallelized; the parallel efficiency is close to unity. All of the simulations reported in this paper were performed on a 40-node DEC-Alpha 4/175 cluster interconnected by two Gigaswitches and on an 8-node DEC-Alpha 5/500 cluster interconnected by FastEthernet in the Concurrent Computing Laboratory for Materials Simulations at Louisiana State University.

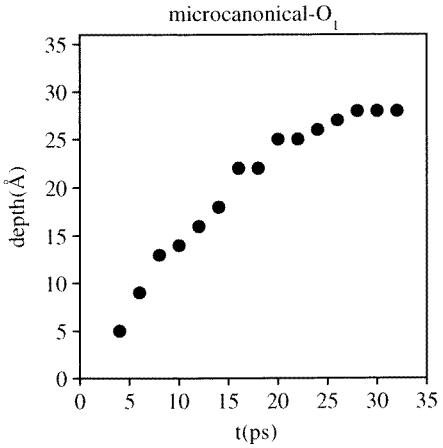

Figure 1. The time evolution of the oxidation depth for the microcanonical O_1 run.

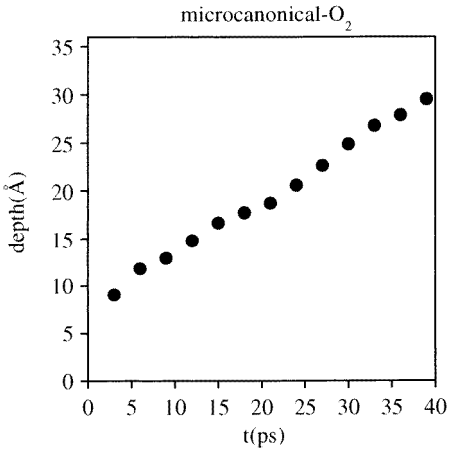

Figure 2. As figure 1, but for the microcanonical O_2 run.

3. The oxidation dynamics of an aluminium nanocluster

3.1. The time evolution of the oxidation depth

Figure 1 depicts the time evolution of the oxidation depth in the microcanonical O_1 run. The depth is defined as the difference between two boundary radii: the outer one corresponds to that where the spherically averaged density of Al takes on a value that is one tenth of its maximum; the inner one is defined in the same way, but for the density of O. Since we calculate the spherically averaged density for every $\delta r = 10$ Å shell, the values of the oxidation depth may contain possible errors of a few Å. As seen in figure 1, the depth increases linearly with time up to 25 Å, reached at $t = 20$ ps; thereafter the rate becomes lower. The saturation depth is $\sim$28 Å.

In experiments, oxidation of Al nanoclusters proceeds in O_2 gas rather than O_1 gas.

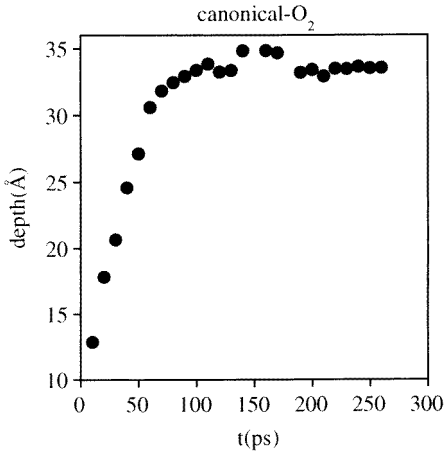

Figure 3. As figure 1, but for the canonical O_2 run.

Also, we have ignored heat transfer due to electrons in the present simulations, which has the effect of lowering the surface temperatures. These facts motivate us to compare the results from the microcanonical O_1 run with those from the canonical and microcanonical O_2 runs. Figure 2 depicts the time evolution of the oxidation depth in the microcanonical O_2 run. In the microcanonical O_2 run, the oxidation depth develops to ∼30 Å at $t = 40$ ps when the centre of the Al core reaches ∼900 K. By comparing figures 1 and 2, we see that inclusion of the O_2-dissociation energy lowers the rate of surface temperature increase and thereby delays the thickening processes of the surface oxides by 30%.

Figure 3 depicts the time evolution of the oxidation depth in the canonical O_2 run. In the canonical O_2 run, the Al core assumes fcc crystalline structure at all times while the surface oxides are melted, with $T = 1500$–2000 K for $t > 40$ ps. The depth increases linearly with time until it reaches about 30 Å, at $t = 60$ ps. Such linearity of the oxidation depth with respect to time in the initial stage has also been observed in the microcanonical O_1 run (see figure 1). The depth of the surface oxides in the canonical O_2 run is saturated at ∼33 Å at $t = 260$ ps as seen in figure 3. The sudden jumps (±1 Å) in the oxidation depth seen in figure 3 are artifacts of the procedure used here to measure the oxidation depth. We note that the saturation depths in all three simulations reside in a narrow range, 28–33 Å, in spite of the significant differences between the states of the oxygens and between the thermodynamic ensembles.

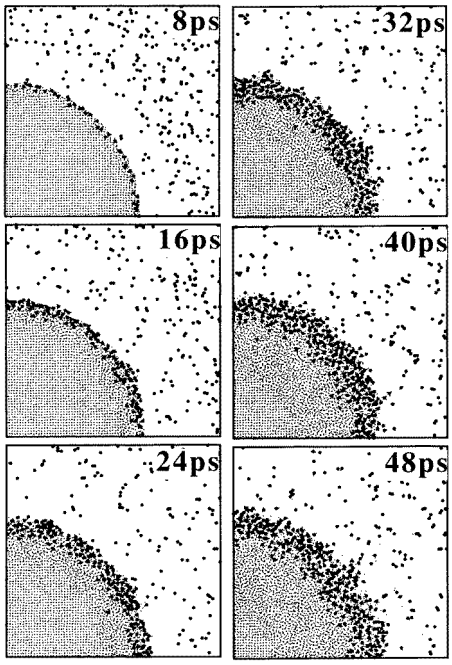

Figure 4. The x–y projection maps of a sheet ($x = 0$–150 Å, $y = 0$–150 Å, $z = 0$–8 Å) at various times in the microcanonical O_1 run. The larger spheres correspond to oxygens, the smaller spheres to aluminiums.

Figure 4 shows x–y projection maps of a sheet ($x = 0$–150 Å, $y = 0$–150 Å, $z = 0$–8 Å) at $t = 8$, 16, 24, 32, 40, and 48 ps in the microcanonical O_1 run. The larger spheres in figure 4 correspond to oxygens, the smaller spheres to aluminiums. The O

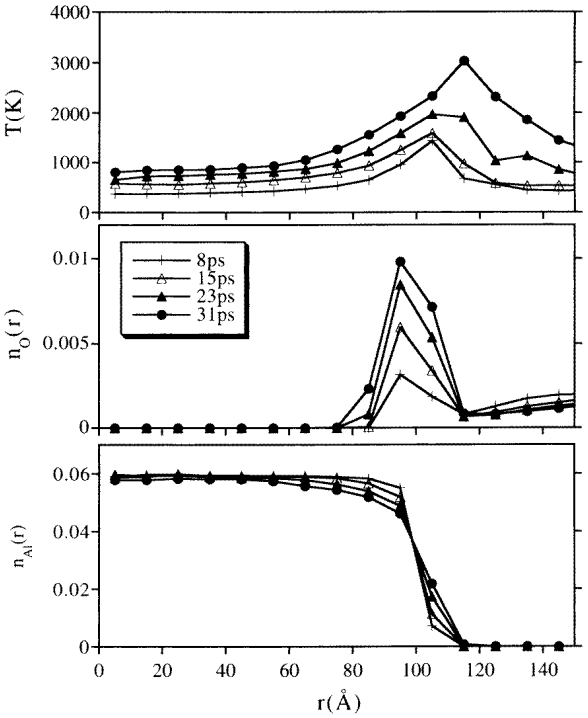

Figure 5. The spherically averaged temperatures and densities of the oxygens and aluminiums at various times for the microcanonical O_1 run.

atoms assume negative charges in the range $-1.0e$ to $-0.5e$ once they are captured on the cluster. Disordering of the crystalline Al core develops from the surface, which extends to $r \sim 50$ Å at $t = 31$ ps as seen in figure 4. This is because crystalline Al melts at high temperatures >1000 K (see figure 5 (top)). The charge density in each 10 Å radial shell is nearly zero, showing the establishing of charge neutrality within short distances (<10 Å). The oxygen atoms in the oxides diffuse predominantly along the surface; their mean square displacements are $\Delta r_t^2/\Delta t \sim 14 \times 10^{-4}$ cm^2 s^{-1} for tangential motions and $\Delta r_r^2/\Delta t \sim 7 \times 10^{-4}$ cm^2 s^{-1} for radial motions at $t = 23$ ps. Radial diffusion of oxygens toward the centre is suppressed because of the lower temperatures at smaller radii. The uniformity in the oxidation depths as regards the polar angles, observed in figure 4, results from such enhanced surface diffusion. For $t > 40$ ps in figure 4, we observe thermal emission of fragmented oxides with various sizes. The surface temperature is higher than 3000 K for $t > 40$ ps as depicted in figure 5 (top). The entire cluster melts at $t \sim 55$ ps.

The time evolution of the local pressure P averaged over 1 ps is also investigated in reference [12] for the microcanonical O_1 run. At $t = 7$–8 ps, the surface region ($r = 90$–100 Å) assumes negative pressures $P = -2$ to -1 GPa while the inner region has nearly zero pressure. This is in accordance with fast increase in the oxidation depth in the initial stage (see figure 5 (top)). Due to the heat transfer from the surface to the core region, in the inner region ($r < 70$ Å) P assumes positive values $\sim$1 GPa at $t = 14$–15 ps. At $t = 22$–23 ps, corresponding to the saturation of the oxidation depth, the boundaries between the negative- and positive-P regions are blurred. These regions mix in a complex manner at $t = 30$–31 ps.

3.2. Time evolution of the local densities and temperatures

Figure 5 shows the time evolution of the spherically averaged temperatures and densities of the oxygens and aluminiums for the microcanonical O_1 run. The density of oxygens in the surface oxides (r = 90–100 Å) increases up to $n_O = 0.010$ Å^{-3} at $t = 31$ ps; correspondingly the density of aluminiums $n_{Al} = 0.046$ Å^{-3}. Hence the ratio $n_O/n_{Al} = 0.21$ in the surface oxides, which is substantially smaller than the value 1.5 for Al_2O_3. At the stage of saturation in the oxidation depths, i.e., for $t \sim 31$ ps, we observe in figure 5 that the oxygens are depleted at r = 115–150 Å and their averaged density is $\sim$0.001 Å^{-3}. Molecular oxides in the form of AlO and Al_2O are known to be stable at high temperatures (>1900 K) [13]. The temperature at $r = 115$ Å, which corresponds to the boundary between the surface oxides and the environment, is in fact around 3000 K at $t = 31$ ps as seen in figure 5 (top). A possible reason for the saturation is that the matter in the depletion region has reached equilibrium at high temperatures.

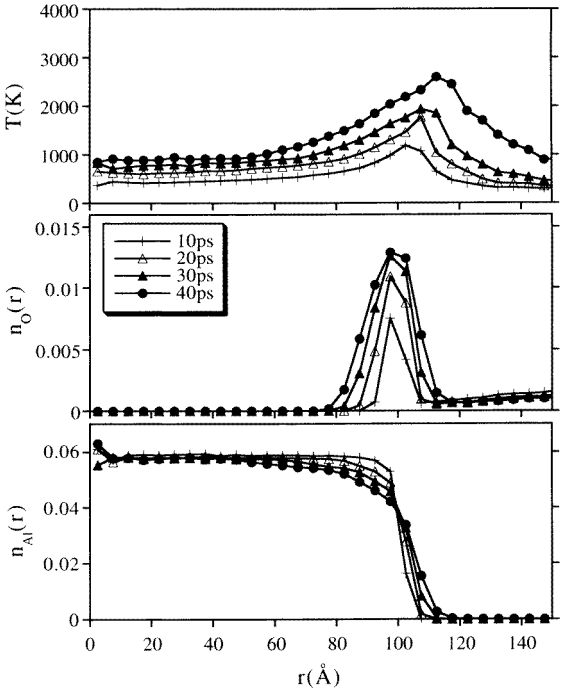

Figure 6. As figure 5, but for the microcanonical O_2 run.

Similar analyses for the time evolution of the spherically averaged temperatures and densities of oxygens and aluminiums were performed for the microcanonical O_2 run; figure 6 depicts these values at t = 10, 20, 30, and 40 ps. In the microcanonical O_2 run, the averaged density of oxygens in the surface oxides is $n_O = 0.013$ Å^{-3} at $t = 40$ ps, which is about 30% larger than that at $t = 31$ ps in the microcanonical O_1 run. Such an increase in the oxygen density results because the Al cluster is exposed to oxygen gas for about 30% longer in the microcanonical O_2 run. The ratio $n_O/n_{Al} = 0.31$ in the oxide (r = 90–100 Å), which is larger than the value 0.21 for the microcanonical O_1 run.

Figure 7 shows the spherically averaged temperatures and densities of the oxygens and aluminiums for the canonical O_2 run at t = 60, 120, 180, and 240 ps. Since the temperature

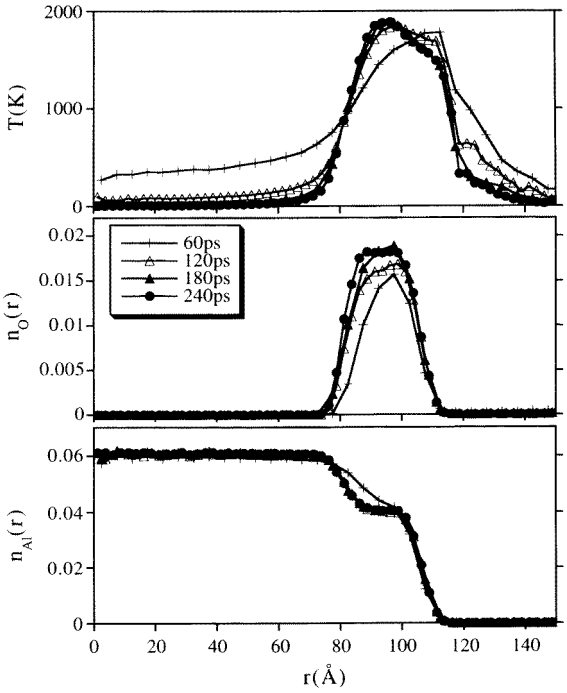

Figure 7. As figure 5, but for the canonical O_2 run.

of the whole system is set to 400 K in the canonical O_2 run, the core region of the Al cluster assumes crystalline structure. The averaged densities of the oxygens in the surface oxides ($r = 80$–100 Å) are $n_O \sim 0.021$ Å^{-3} and $n_{Al} \sim 0.041$ Å^{-3} at $t = 260$ ps in the canonical O_2 run. Hence the ratio $n_O/n_{Al} = 0.51$ is substantially larger than that for the microcanonical O_2 run.

4. Vibrational properties of the amorphous surface oxides

The depths of the surface oxides as a function of the radius of the Al nanocluster have been estimated in experiments [4]. The depth is ∼30 Å for the cluster with the radius 100 Å [4]. The microscopic structures of the oxides are unknown. Despite orders of magnitude difference in the oxygen gas density, a remarkable similarity in the oxidation depth is found between the present results and the experimental observation. We therefore quenched the molten surface oxides obtained in the canonical O_2 run to obtain amorphous surface oxides for the structure analyses. We take the atomic configuration at $t = 260$ ps in the canonical O_2 run and supply O_2 molecules in the environmental region ($r > 120$ Å) to achieve $n_O = 0.0020$ Å^{-3}. Using a Nosé–Hoover thermostat [9], we then gradually quenched the temperature of the whole system toward 0 K for $t = 260$–452 ps. In the quenching sequence, we paused the run five times to add O_2 molecules, with the intention of maintaining $n_O(r = 400$ Å$)$ between 0.001 and 0.002 Å^{-3}.

As a result, amorphous surface oxides with mean depth ∼38 Å were formed as shown in figure 8. The figure is an x–y projection map of the quenched cluster ($x = 0$–120 Å, $y = 0$–120 Å, $z = 0$–8 Å). The larger spheres in figure 8 correspond to oxygens; smaller spheres

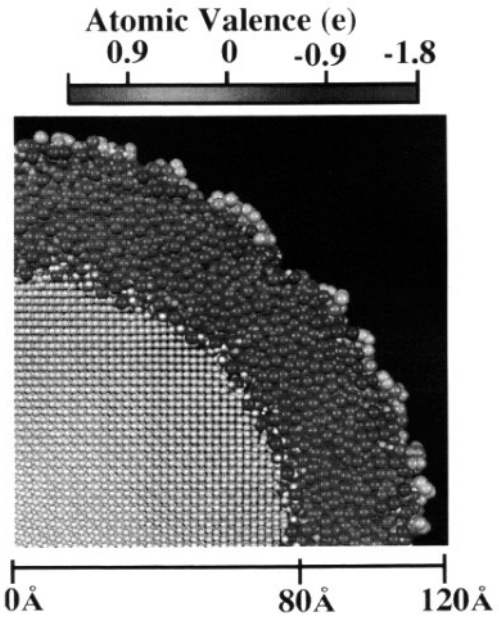

Figure 8. The x–y projection map of a sheet (x = 0–120 Å, y = 0–120 Å, z = 0–8 Å) for the quenched cluster. The larger spheres correspond to oxygens, the smaller spheres to aluminiums.

correspond to aluminiums. Their mean densities in the surface oxides are $n_O = 0.041$ Å^{-3} and $n_{Al} = 0.043$ Å^{-3}; the mean charges are $q_O = -1.43e$ and $q_{Al} = 1.37e$. Therefore the mass density of the surface oxides is $\sim$3.0 g cm^{-3}, which is smaller than the value 4.0 g cm^{-3} for α-Al_2O_3.

Figure 9 (top) compares the vibrational densities of states (DOSs) for various radial shells of the quenched cluster. They are obtained by Fourier transforming the velocity autocorrelation functions of the atoms. The DOSs for the oxides are compared with the DOSs for crystalline Al and α-Al_2O_3. We remark that the DOS for the crystalline Al is indistinguishable from that for the Al nanocluster with r = 100 Å. The DOS for the crystalline Al has the range $E = \hbar\omega$ = 10–40 meV, while the DOS for α-Al_2O_3 has ranges in two bands: E = 20–70 meV and 90–110 meV. The prominent peaks at E = 17 and 35 meV observed for the 60–70 Å shell in figure 9 (top) are common to crystalline Al, as seen in figure 9 (bottom). The energy range of the DOS extends to E = 10–120 meV for the 70–80 Å shell. The DOS for the surface oxides (80–110 Å) has two broad bands centred at E = 40 and 90 meV, whose corresponding structures are found in the DOS for α-Al_2O_3 in figure 9 (bottom).

Further analyses on the microscopic structures of the amorphous surface oxides are performed in reference [12] through coordination numbers and bond angles. We define the nearest neighbours of an atom as those particles with separation distances smaller than 2.5 Å, which corresponds to the first minimum of the radial distribution function of O atoms around an Al atom. The coordination number N_c of an atom is obtained as the number of its nearest-neighbour atoms of various different species. We thereby find that both Al and O atoms have N_c = 3–5 in the oxides. In the larger-r shell (r = 100–110 Å) of the oxide, N_c = 4–5 for Al and N_c = 3–4 for O atoms. Through the distribution of the angle θ between two connecting lines originating from an O atom and going to its nearest-neighbour

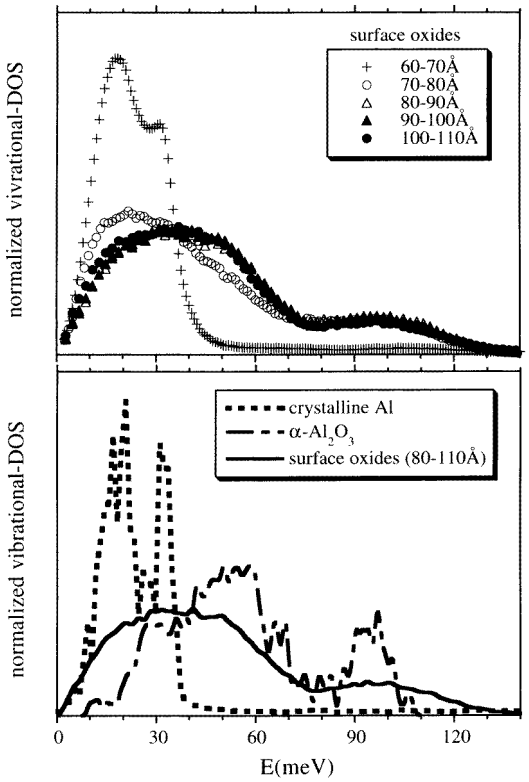

Figure 9. Top: normalized vibrational DOSs for various radial shells of the quenched cluster. Bottom: comparison of the DOSs for the surface oxides of the quenched cluster, crystalline Al, and α-Al_2O_3.

Al atoms, we find that the angle θ_{max} at which the distribution reaches its maximum is $\sim 105^\circ$ for the outer region (90–110 Å) and $\theta_{max} \sim 90^\circ$ for the inner region (70–90 Å). The angle 105° is close to 109°, corresponding to a tetrahedron, $(Al_{1/4})_4O$; the angle 90° corresponds to an octahedron, $(Al_{1/6})_6O$. For α-Al_2O_3 crystal, which is made of distorted octahedrons, $(Al_{1/6})_6O$, $N_c = 6$ for Al and $N_c = 4$ for O atoms [14]. $N_c = 4$ or 6 for Al and $N_c = 3$ or 4 for O atoms for γ-Al_2O_3 crystal [15], whose principal local structure is distorted $(Al_{1/4})_4O$. In the outer region (90–110 Å) of the oxides, local structures around O atoms therefore resemble those for γ-Al_2O_3, though the ratio $n_O/n_{Al} \sim 0.95$ for the oxides is smaller than the value 1.5 for Al_2O_3. We may regard the local structures in the inner region (70–90 Å) as mixtures of $(Al_{1/3})_3O$, $(Al_{1/4})_4O$, $(Al_{1/5})_5O$, and $(Al_{1/6})_6O$ structures.

5. Summary

We have performed variable-charge MD simulations for the oxidation of an Al nanocluster in oxygen gas. The oxidation depths have been saturated at $\sim$30 Å, depending weakly on the setting of the simulation. The surface oxides have melted due to their high temperatures, caused by the energy release in the oxidation reaction. The saturation behaviour in the oxidation depth has resulted from depletion of oxygen atoms in the surrounding region near the surface of the cluster. Such depletion may be related to the formation of the stable

molecules AlO or Al_2O at high temperatures (>1900 K). By further quenching the cluster in oxygen gas, we formed amorphous surface oxides with depths ∼38 Å. The microscopic structures of the amorphous surface oxides were investigated through the vibrational DOSs, and bond analyses.

Acknowledgments

The simulations were performed in collaboration with Drs K Tsuruta, A Nakano, R K Kalia, and P Vashishta in the Concurrent Computing Laboratory for Materials Simulations at Louisiana State University. This work was supported by the Ministry of Education, Science, and Culture of Japan, the US Department of Energy, the National Science Foundation, the Air Force Office of Scientific Research, the Army Research Office, the Louisiana Education Quality Support Fund, the USC–LSU Multidisciplinary University Research Initiative, and the Petroleum Research Fund. The facilities in the Concurrent Computing Laboratory for Materials Simulations were acquired with the Equipment Enhancement Grants awarded by the Louisiana Board of Regents through Louisiana Education Quality Support Fund. One of us (TJC) is supported by a NSF Graduate Research Traineeship.

References

[1] See, e.g.,
Askeland D R 1989 *The Science and Engineering of Materials* (Boston, MA: PWS-KENT) ch 20
[2] For a theoretical consideration of the mechanism, see
Mott N F 1939 *Trans. Faraday Soc.* **35** 1175
Cabrera N and Mott N F 1949 *Rep. Prog. Phys.* **12** 163
[3] Shinohara K, Seo T and Kyogoku H 1982 *Z. Metallk.* **73** 774
[4] Sako S, Ohshima K and Fujita T 1990 *J. Phys. Soc. Japan* **59** 662
[5] Aumann C E, Skofronick G L and Martin J A 1995 *J. Vac. Sci. Technol.* B **13** 1178
[6] Suits B H, Apte P, Wilken D E and Siegel R W 1995 *Nanostruct. Mater.* **6** 609
[7] See, e.g.,
Nakano A, Bachlechner M E, Campbell T J, Kalia R K, Omeltchenko A, Tsuruta K, Vashishta P, Ogata S, Ebbsjö I and Madhukar A 1998 *IEEE Comput. Sci. Eng.* submitted
[8] Tuckerman M, Berne B J and Martyna G J 1992 *J. Chem. Phys.* **97** 1990
[9] Martyna G J, Tuckerman M E, Tobias D J and Klein M L 1996 *Mol. Phys.* **87** 1117
[10] Streitz F H and Mintmire J W 1994 *Phys. Rev.* B **50** 11 996
[11] Greengard L and Rokhlin V 1987 *J. Comput. Phys.* **73** 325
[12] Ogata S, Campbell T J, Tsuruta K, Nakano A, Kalia R K and Vashishta P 1998 in preparation
[13] Hoch M and Johnson H L 1954 *J. Am. Chem. Soc.* **76** 2560
Brewer L and Searey A W 1951 *J. Am. Chem. Soc.* **73** 5308
[14] Wyckoff R W G 1964 *Crystal Structures* 2nd edn, vol 2 (New York: Interscience) ch 5
[15] See, e.g.,
Alvarez L J, Sanz J F, Capitan M J and Odriozola J A 1992 *Chem. Phys. Lett.* **192** 463